# Phase Behavior of Ordered Diblock Copolymer Blends: Effect of Compositional Heterogeneity

**Richard J. Spontak,*,† Jennifer C. Fung,‡ Michael B. Braunfeld,§ John W. Sedat,§ David A. Agard,§ Lisaleigh Kane,† Steven D. Smith,*,|| Michael M. Satkowski,|| Arman Ashraf,|| Damian A. Hajduk,⊥,¶ and Sol M. Gruner⊥**

*Department of Materials Science and Engineering, North Carolina State University, Raleigh, North Carolina 27695, Graduate Group in Biophysics, University of California, San Francisco, California 94143, Department of Biochemistry and Biophysics and the Howard Hughes Medical Institute, University of California, San Francisco, California 94143, Corporate Research Division, The Procter & Gamble Company, Cincinnati, Ohio 45239, and Department of Physics, Princeton University, Princeton, New Jersey 08544*

*Received October 24, 1995; Revised Manuscript Received January 17, 1996*[⊗]

ABSTRACT: Diblock copolymers order into a variety of periodic morphologies when the constituent blocks are sufficiently incompatible. Previous studies have demonstrated that classical dispersion (spherical and cylindrical) and lamellar morphologies, as well as complex morphologies (*e.g.*, gyroid*, lamellar catenoid, and hexagonally perforated lamellae), can be selectively accessed through either tailored molecular synthesis or copolymer/homopolymer blends. In the present work, control over ultimate morphology is achieved through the use of binary copolymer blends composed of two strongly-segregated poly(styrene-*b*-isoprene) (SI) diblock copolymers of equal molecular weights but different compositions (one 50 wt % S and the other 85 wt % S). Blend morphologies are examined by electron microscopy (including three-dimensional imaging) and small-angle X-ray scattering, and a theoretical framework is proposed to describe strongly-segregated copolymer blends exhibiting the lamellar morphology. Results obtained here indicate that diblock copolymer blends of a given bulk composition may exhibit coexisting morphologies but in general behave as single-phase diblock copolymers of equal molecular composition, suggesting that such blends offer an alternative, and attractive, route by which to generate a desired morphology.

## Introduction

Neat AB diblock copolymers undergo self-organization when the contiguous A and B monomer sequences are sufficiently incompatible, that is, when $\chi N \rightarrow (\chi N)_{ODT}$, where $\chi$ is the Flory−Huggins interaction parameter, $N$ is the number of statistical units along the backbone, and the subscript denotes the order−disorder transition (ODT).[1] For $\chi N > (\chi N)_{ODT}$, the copolymer orders into a variety of periodic morphologies, depending on factors such as thermodynamic incompatibility ($\chi N$), molecular composition ($f$), and statistical segment length asymmetry.[2−4] Classical diblock copolymer morphologies include spheres of A (or B) arranged on a body-centered cubic (bcc) lattice in a matrix of B (or A), hexagonally packed cylinders of A (or B) in a matrix of B (or A), and alternating lamellae of A and B. More complex morphologies, such as the lamellar-catenoid/hexagonally perforated lamellar (LC/HPL)[5−7] and gyroid* (G*)[7−9] morphologies, have also been observed in neat diblock copolymers[10] and, more recently, in linear multiblock copolymers.[11] These "nonclassical" bicontinuous morphologies appear over narrow composition ranges separating the lamellar and cylindrical morphologies.

Efforts designed to establish molecule-morphology relationships in diblock copolymers have traditionally relied on model materials with highly tailored compositions and molecular weights. Synthesis of neat copolymers possessing particular compositions for morphological studies or morphology-specific applications is, however, laborious and, in many cases, not commercially viable. Several studies[12−16] have successfully shown that a desired morphology can be more readily generated by blending a diblock copolymer with a parent homopolymer. Blends of a lamellar poly(styrene-*b*-isoprene) (SI) copolymer and homopolystyrene (hS) have, for instance, yielded lamellae, a cubic bicontinuous morphology,[10] ordered cylinders/spheres, and disordered micelles, depending on blend composition. More recent studies have shown that additional nonclassical morphologies, such as the LC[16−18] and G*,[8] can be produced in the same fashion.

In essence, blending facilitates control over ultimate morphology by permitting continuous alteration of the minority component volume fraction. However, in copolymer/homopolymer blends, the mobility of the homopolymer residing within microdomains of the chemically identical block requires that homopolymer localization must also be considered. Theoretical frameworks[19−21] predict that the distribution of homopolymer A (hA) within an AB diblock lamellar morphology reaches a maximum near the center of each A microdomain, with the extent of localization depending on the molecular weight of hA relative to that of the host A block. Similar restrictions are believed to occur in nonlamellar morphologies, in which hA partitions into regions of the unit cell to relieve the stress associated with A-block stretching.[8] Although direct experimental confirmation of such localization has not been achieved in block copolymer melts, it has been observed[22] in nonlamellar morphologies of certain phospholipid−water systems.

* To whom correspondence should be addressed.
† North Carolina State University.
‡ Graduate Group in Biophysics, University of California.
§ Department of Biochemistry and Biophysics and the Howard Hughes Medical Institute, University of California.
|| The Procter & Gamble Co.
⊥ Princeton University.
¶ Present address: Department of Chemical Engineering and Materials Science, University of Minnesota, Minneapolis, MN 55455.
⊗ Abstract published in *Advance ACS Abstracts,* April 15, 1996.

S0024-9297(95)01568-3 CCC: $12.00 

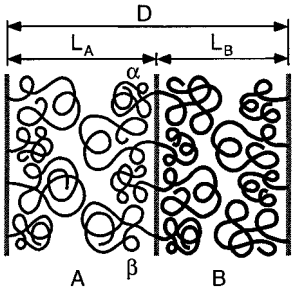


**Figure 1.** Schematic depiction of the lamellar morphology illustrating the chain placement and packing of a miscible copolymer/copolymer blend in which the constituent AB diblock copolymers possess different compositions but identical chain lengths ($N_\alpha = N_\beta$). By arbitrary convention, the A block of the α copolymer is shorter than that of the $\beta$ copolymer (i.e., $f_{A,\alpha} < f_{A,\beta}$). Also shown here are the microdomain thickness ($L_i$, i = A or B) and periodicity ($D$).

Replacement of hA by a second strongly-segregated diblock copolymer forces one of the "homopolymer" chain ends in each A microdomain to locate in the AB interfacial region (see Figure 1) and introduces a similarly restricted B block into each B microdomain. Due to variations about the mean A and B block lengths in their respective microdomains, the ultimate morphology in such copolymer/copolymer blends is anticipated to be highly sensitive to chain packing and, hence, to the distribution of chain lengths within the blend. Since all of the copolymer molecules in such blends are anchored during microphase ordering, the morphologies generated in copolymer/copolymer blends are expected[23] to be more representative of those found in neat copolymers (of equal bulk composition) than those obtained in binary copolymer/homopolymer blends.

In this work, we examine the phase behavior of a series of copolymer/copolymer blends and explore the possibility of using blending[24] to tailor ultimate morphology. The blend morphologies produced here are characterized by transmission electron microscopy (TEM), intermediate voltage electron microscopic tomography (IVEM-T), and small-angle X-ray scattering (SAXS). We also describe a strong-segregation theoretical framework which addresses the microdomain characteristics of lamellar copolymer blends.

## Experimental Section

Two SI diblock copolymers were synthesized *via* living anionic polymerization in cyclohexane at 60 °C. The initiator in each case was *sec*-butyllithium. According to proton nuclear magnetic resonance ($^1$H NMR), one of the copolymers (α) was symmetric (50 wt % S), while the other ($\beta$) was asymmetric (85 wt % S). Both copolymers possessed number-average molecular weights of 80 000 and polydispersities of approximately 1.04, as discerned by gel permeation chromatography (GPC). The mass of the S block in each copolymer was first measured by GPC upon consumption of all styrene monomer, and the mass of each I block was then determined from a combination of the overall $\bar{M}_n$ (GPC) and the molecular composition ($^1$H NMR). Physical blends were prepared in increments of 10 wt % α, ranging from pure α to pure $\beta$, and are designated hereafter by $X/(100 - X)$ α/$\beta$, where $X$ denotes the wt % of α. Films of the two copolymers and their blends were prepared from 5% (wt/v) solutions in toluene according to an earlier protocol for copolymer/homopolymer blends.[16] Upon slow solvent removal over the course of 3 weeks at ambient temperature and extensive annealing for 1 week at *ca.* 160 °C (which is well above the upper, styrenic, glass transition temperature in each parent copolymer), the films, measuring about 2 mm thick, were presumed to be near-equilibrium.

Electron-transparent specimens for TEM were obtained by sectioning the center of each film normal to the film surface at −100 °C in a Reichert-Jung Ultracut-S cryoultramicrotome. The resulting specimens were stained for 90 min with $OsO_4$ vapor from a 2% aqueous solution and examined using Zeiss EM902, Philips 430, and JEOL 200CX electron microscopes, operated at 80, 200, and 120 kV, respectively. Correlation maxima corresponding to reciprocal microdomain periods were measured from digitized electron micrographs upon Fourier transformation with Digitalmicrograph software (Gatan Inc., Pleasanton, CA). Three-dimensional reconstructions from IVEM-T data were obtained using a combination of customized and commercial software running on Silicon Graphics workstations (described later). Small-angle X-ray scattering was performed at Procter & Gamble with Cu Kα radiation ($\lambda$ = 0.154 nm) generated from a Rigaku RU-300 rotating anode X-ray diffractometer operated at 40 kV and 200 mA with Kratky optics. Resulting patterns were not desmeared. Analogous measurements performed at Princeton University employed a Rigaku RU-200BH rotating anode instrument equipped with a 0.2 × 0.2 mm$^2$ microfocus cathode and Franks mirror optics. Samples were mounted inside an evacuated sample chamber and maintained at the temperature of interest by a set of thermoelectric devices with a temperature range of 0−185 °C and stability about the setpoint of ±0.05 °C. Two-dimensional diffraction images were collected with an image-intensified area detector designed around a Thompson CCD chip. After collection, images were digitized, corrected for detector response characteristics, and written to magnetic tape. Images were collapsed into a one-dimensional format by integrating azimuthally along an arc ±15° from the horizontal axis.

## Results and Discussion

**I. Neat Copolymer Phase Behavior.** According to mean-field considerations,[1] the position of neat SI diblock copolymers in phase space is determined by thermodynamic incompatibility ($\chi N$) and volume-fraction composition ($f_S$). In SI block copolymer blends, the bulk volume fraction of S ($\langle f_S \rangle$) provides a measure of the sample composition,[14,15] which can be calculated from the known composition of the blend components, the concentration ($X$) of each in the blend, and the densities of polystyrene ($\rho_S$) and polyisoprene ($\rho_I$). We evaluate $f_S$ and $\langle f_S \rangle$ at ambient temperature ($\rho_S$ = 1.05 g/cm$^3$ and $\rho_I$ = 0.91 g/cm$^3$) and at the polystyrene glass transition temperature ($\rho_S$ = 1.00 g/cm$^3$,[25] and $\rho_I$ = 0.84 g/cm$^3$,[26] at 100 °C). Corresponding values of $f_S$ for the parent copolymers (denoted α and $\beta$, $f_S$ = 0.46 for α and 0.83 for $\beta$) suggest that these materials possess lamellar and spherical morphologies, respectively.

Since $\chi$ and $N$ are not expected to differ substantially for the two parent copolymers, the thermodynamic incompatibility can, for all practical purposes, be considered nearly constant throughout the present blend series. Due to uncertainty associated with the *a priori* calculation of $\chi N$, the degree of block copolymer segregation (i.e., weak, intermediate and strong) can be more generally described[27,28] in terms of the scaling behavior of microstructural dimensions (e.g., the microdomain periodicity) with respect to molecular weight, rather than by $\chi N$. Since the α and $\beta$ copolymers employed here possess identical molecular weights, however, such analysis is not of value in the present study. Thus, on the basis of the molecular weights of the polymers, we expect that the neat α and $\beta$ copolymers, as well as their blends, reside within either the intermediate- or strong-segregation regimes.

**II. Blends Possessing the Lamellar Morphology. A. Experimental Observations.** Figure 2 is a series of four SAXS profiles obtained from the 100/0, 90/10, 80/20, and 70/30 $(SI)_\alpha/(SI)_\beta$ blends in which $Iq^2$ is plotted against $q$, where $I$ is scattering intensity and $q$ denotes scattering vector. All of these profiles reveal that (i)

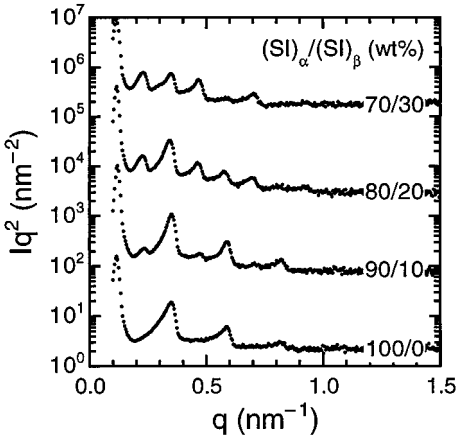


**Figure 2.** Small-angle X-ray scattering profiles ($Iq^2$ *vs* $q$, where $I$ denotes scattering intensity and $q$ is the scattering vector) collected from α/$\beta$ blends ranging in $X$ from 100% (bottom) to 70% (top) in 10% increments. From the peak spacing ratios, these α-rich blends exhibit the lamellar morphology. As in subsequent figures, the blend profiles are shifted vertically to facilitate peak discrimination.

the blends possess the lamellar morphology, since the peaks are equally spaced, and (ii) the lamellar microdomains possess reasonable long-range order, as evidenced by up to 7 orders of reflections. Note that the position of the first (maximum) scattering peak ($q^*$) is relatively close to the beamstop, near the left edge of each profile (at approximately 0.12 $nm^{-1}$). Since $q^*$ provides a measure of the microdomain periodicity ($D = 2\pi/q^*$, by Bragg's law), it is interesting to note that $q^*$ remains virtually invariant in this series of blends, a feature which is consistent with the predicted[29,30] composition independence of $D$ for neat lamellar copolymers. In the α copolymer, only the odd reflections are visible due to the compositional symmetry of the molecule.[31] As $\beta$ copolymer is added, the even reflections are observed to increase gradually in scattering intensity as $\langle f_S \rangle$ deviates from 0.5. The peak intensities and spacings appear to be well-behaved to 80/20 α/$\beta$. In the profile corresponding to the 70/30 blend, however, the fifth reflection is not very pronounced, even though the sixth reflection clearly remains.

Electron micrographs of the four blends used to produce Figure 2 are displayed in Figure 3 and reveal that classical morphologies are present in only some of these blends. Alternating lamellae constitute the single microstructure observed in the pure α copolymer (Figure 3a) and the 90/10 blend (Figure 3b). While lamellar microdomains (verified through tilting) are predominant in the 80/20 blend (Figure 3c), Figure 3d reveals that small patches of dispersed isoprenic cylinders are also evident. The absence of diffraction characteristic of cylinders from the data in Figure 2 suggests that these cylinders occupy only a small fraction of the sample volume. The demarcation from lamellar to cylindrical microstructure appears to be gradual and is reminiscent of the lamellar → cylindrical order−order transition reported by Hajduk *et al.*[32] Note that the cylinders possess a noticeably larger cross-section than the isoprenic lamellae, which is consistent with the equilibrium coexistence of two dissimilar morphologies.

According to Matsen and Bates,[23] relatively broad morphology coexistence regions are stable between the lamellar and hexagonal morphologies in binary blends of diblock copolymers of equal $N$ and different compositions. Unlike typical micrographs of macrophase-separated diblock copolymer blends,[33] though, the regions of cylindrical microstructure in Figure 3 tend to be small, sometimes consisting of less than 10 microdomains along a lamellar row (see Figure 3d). In some cases, single cylindrical microdomains residing in a lamellar matrix have been observed. Assuming narrow interfacial regions,[29] calculation of $\langle f_S \rangle$ from these micrographs ($\langle f_S \rangle = L_S/D$, where $L_S$ denotes the width of the styrenic lamellae) yields styrenic volume fractions (±0.04) of 0.51 (100/0), 0.55 (90/10), and 0.58 (80/20). Corresponding estimates of $\langle f_S \rangle$ obtained from the bulk composition of the blend are in reasonably good agreement with these values (0.46, 0.50, and 0.53, respectively). It should be noted, however, that the S lamellae in close proximity to regions comprised of cylindrical microdomains appear broader than those that are representative of the blends.

In the 70/30 blend (Figure 3e,f), lamellar and cylindrical morphologies coexist. At this composition, the grains of dispersed cylinders (see Figure 3e) appear larger than those seen in the 80/20 blend (Figure 3d). Existence of dispersed cylinders in the 80/20 and 70/30 blends is unexpected and, indeed, somewhat surprising, since the lamellar and cylindrical morphologies are presumed to be separated by an ordered bicontinuous morphology of intermediate interfacial curvature and interfacial packing density.[8,14−16] Some features of the 70/30 blend morphology do, however, suggest that the morphology exhibits characteristics of both coexisting phases. For example, the micrograph presented in Figure 3f demonstrates that the microstructure present in this blend is capable of producing a relatively large $s = +1/2$ disclination, which is commonly seen in lamellar copolymers and copolymer blends. Upon close examination of Figure 3f, it is immediately clear that the microstructural elements responsible for this disclination are neither lamellar nor cylindrical, but belong to an intermediate (and, as of yet, unidentified) morphology. Another possibility is that the morphologies produced in the 80/20 and 70/30 blends are not representative of a narrow thermodynamically-driven coexistence region, but instead reflect kinetically trapped nonequilibrium microstructures. In the absence of a thermotropic phase transition in a given material, it is difficult to discern conclusively whether a given morphology is representative of equilibrium. Alternatively, if the coexisting microstructures are, in fact, at local equilibrium, the slightly different ratios of the two copolymer species which they would therefore contain might reflect imperfect mixing of the α and $\beta$ copolymers during sample preparation, rather than thermodynamically-driven macrophase separation. Once microphase separation has occurred, redistribution of the α and $\beta$ copolymers to eliminate inhomogeneities in concentration might be extremely slow in nonlamellar morphologies due to the transport of minority component blocks through the majority component domains. The structures observed in this case might then be in equilibrium as far as the *local* concentration of both diblock species is concerned; they would, however, be nonequilibrium in nature when the *global* free energy of the system is considered. We believe that, based on the well-developed long-range order exhibited by other blends in this series, the thorough mixing, solvent removal, and extensive annealing protocol employed during sample preparation results in near-equilibrium copolymer and blend morphologies. However, we recognize that we are unable to *prove* that this is indeed the case, and so we refrain from claiming at this time that we have identified biphasic regions in these binary diblock blends.[34]

**B. Theoretical Considerations.** Several theoretical formalisms capable of predicting the equilibrium

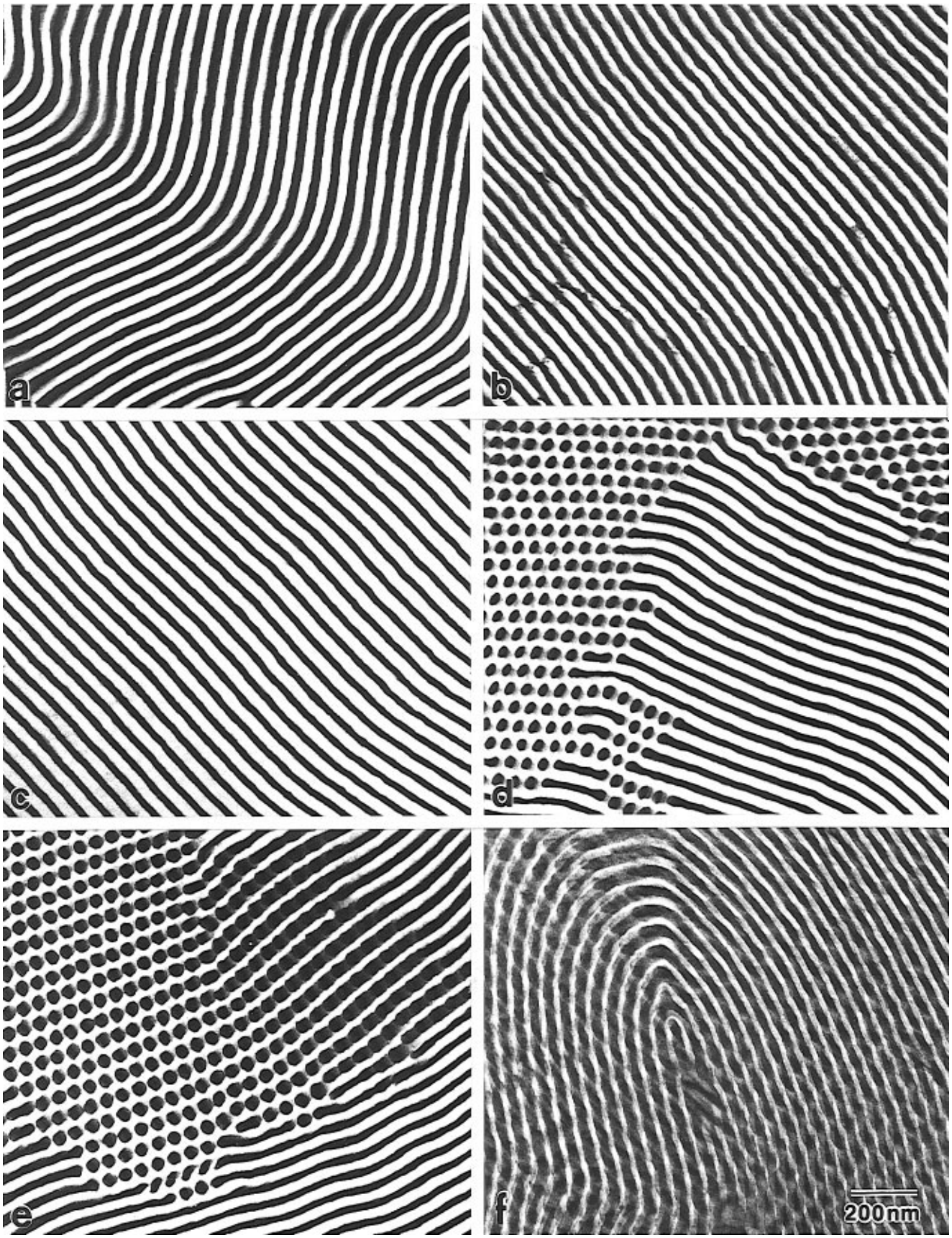


**Figure 3.** Series of transmission electron micrographs obtained from the same α-rich blends described in Figure 2. The 100/0 and 90/10 blends (a and b, respectively) clearly possess the lamellar morphology, while the 80/20 (c and d) and 70/30 (e and f) blends consist of lamellae and discrete grains of isoprenic cylinders. In (f), the 70/30 blend exhibits a relatively large $s = +1/2$ disclination. The isoprenic microdomains appear dark due to selective $OsO_4$ staining.

microdomain characteristics of copolymer/copolymer blend morphologies have recently been proposed.[35−39] One[37] of these extends the previous strong-segregation theories developed for neat diblock[30] and triblock[40,41] copolymers to include binary blends composed of lamellar diblock copolymers with equal (but not necessarily symmetric) compositions. A comparable formalism, as well as a self-consistent field (SCF) framework to

account for intermediate segregation in lamellar diblock copolymer blends, has also been presented by Matsen.[39] In this section, a strong-segregation framework is developed to address lamellar blends in which the constituent copolymers differ in composition, such as the ones presently examined and those investigated by Vilesov *et al.*,[42] so that predictions may assist in explaining the data in Figures 2 and 3.

In this framework, each lamellar microdomain is comprised of both α and $\beta$ A (or B) monomers. Using the entropic expression suggested by Matsen[39] to describe stretching of the mixed α and $\beta$ blocks along the lamellar normal and the narrow interphase approximation[29] to account for interfacial repulsion in the strong-segregation limit (while neglecting the entropy change due to *intra*lamellar mixing), the free energy per area ($F$) can be written as

$$\frac{F}{kT} = \frac{\pi^2}{4b^2}\left(\frac{H_A{}^3\psi_A}{N_{A,\beta}{}^2} + \frac{H_B{}^3\psi_B}{N_{B,\alpha}{}^2}\right) + 2b\left(\frac{\chi}{6}\right)^{1/2} \qquad (1)$$

where $k$ is the Boltzmann constant, $T$ denotes absolute temperature, $b$ is the monomer length (assuming $b_A = b_B$), $H_i$ is the half-width of the ith lamella ($L_i = 2H_i$ in Figure 1), and $N_{i,j}$ is the number of monomers in the ith block (i = A or B) of the jth copolymer (j = α or $\beta$). Note that the $N_{i,j}$ are expressed in terms of the dominant block in the A and B microdomains. The factors $\psi_A$ and $\psi_B$ are given by

$$\psi_A = \frac{R_A + (1 - R_A)(1 - x)^3}{[R_A + (1 - R_A)(1 - x)]^3} \qquad (2a)$$

$$\psi_B = \frac{R_B + (1 - R_B)x^3}{[R_B + (1 - R_B)x]^3} \qquad (2b)$$

where $R_A = f_{A,\alpha}/f_{A,\beta}$ and $R_B = f_{B,\beta}/f_{B,\alpha}$, $f_{i,j}$ is the monomer (volume) fraction of i monomers in the jth copolymer ($f_{A,j} + f_{B,j} = 1$), and $x$ is the mole fraction of α copolymer. In the specific case of constant chain length (i.e., $N_\alpha = N_\beta = N$), the mole fraction of α is equal to the mass fraction of α, and the total number of i monomers (i = A or B) occupying $H_i$ is $N_i = \bar{f}_i N_\alpha$, where $\bar{f}_i = xf_{i,\alpha} + (1 - x)f_{i,\beta}$. From volume-filling considerations, it readily follows that $H_B = H_A\bar{f}_B/\bar{f}_A$ and $D = 2H_A/\bar{f}_A$.

Substitution of these relationships into eq 1, followed by algebraic manipulation, yields the free-energy density ($F$), *viz.*,

$$\frac{F}{kT} = \frac{\pi^2 D^2 \Psi}{32b^2N^2} + \frac{2b}{D}\left(\frac{\chi}{6}\right)^{1/2} \qquad (3)$$

where $\Psi = \psi_A\bar{f}_A{}^3/f_{A,\beta}{}^2 + \psi_B\bar{f}_B{}^3/f_{B,\alpha}{}^2$. Evaluation of $dF/dD = 0$ provides the equilibrium lamellar period ($D_{\alpha\beta}$) as a function of both blend ($x$) and molecular ($f_{i,j}$) compositions:

$$D_{\alpha\beta} = \frac{4}{\sqrt{6}}\left(\frac{3}{\pi^2}\right)^{1/3} bN^{2/3}\chi^{1/6}\Psi^{-1/3} \qquad (4)$$

Equation 4 closely resembles the expression derived[30] for the equilibrium period of either α or $\beta$ lamellar copolymer ($D_\alpha = D_\beta$), in which case $D_r$ for a blend of lamellar copolymers with equal $N$ can be defined as $D_{\alpha\beta}/D_\alpha$ (or $D_{\alpha\beta}/D_\beta$) so that $D_r = \Psi^{-1/3}$. Note that as $x \to 0$ or $x \to 1$, $\Psi \to 1$ and $D_r \to 1$, which is consistent with the result[29,30] that $D$ is independent of molecular composition for neat lamellar diblock copolymers in the strong-segregation regime. Since $D$ from volume and mass conservation is equal to $2H_A/\bar{f}_A$, an analogous expression

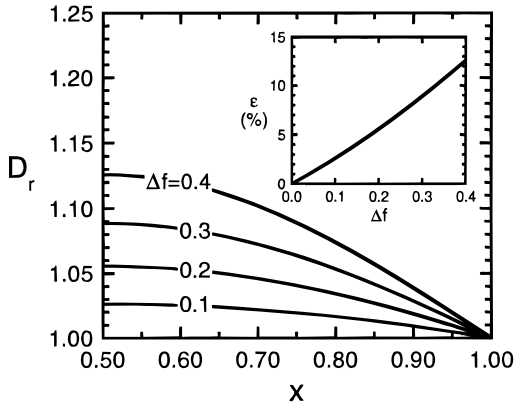


**Figure 4.** Predicted dependence of the reduced blend periodicity ($D_r$) on blend composition ($x$) for different copolymer asymmetries ($\Delta f = f_{A,\beta} - f_{A,\alpha}$, where, by convention, $f_{A,\alpha} < f_{A,\beta}$) in the strong-segregation limit. Maxima in $D_r$ at $x = 0.5$ ($\epsilon$) are presented as a function of $\Delta f$ in the inset.

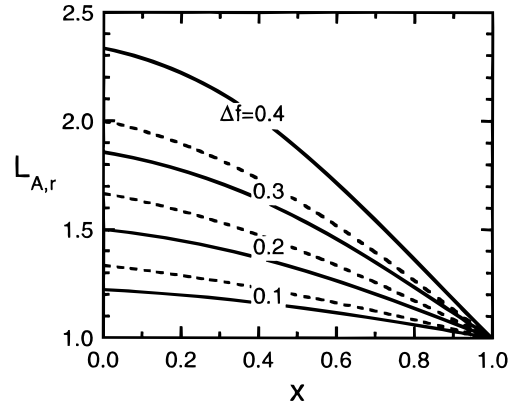


**Figure 5.** Predicted $L_{A,r}(x)$ for the two case examples described in the text. Type (i) blends (with $f_{A,\alpha} + f_{A,\beta} = 1$) are shown as solid lines, while type (ii) blends (with $f_{A,\alpha} = 0.3$) are displayed as dashed lines, for the same $\Delta f$.

for the thickness of an A lamella in the blend, relative to that of the neat α copolymer, can be written as $L_{A,r} = \bar{f}_A D_r/\bar{f}_{A,\alpha}$.

Predicted $D_r$ and $L_{A,r}$ are displayed as functions of blend composition ($x$) in Figures 4 and 5 for two case examples: (i) blends in which $f_{A,\alpha} + f_{A,\beta} = 1$ and (ii) blends with $f_{A,\alpha}$ held constant at 0.3. To facilitate comparison of these cases, blends are classified according to $\Delta f$, where $\Delta f = f_{A,\beta} - f_{A,\alpha}$ (recall from Figure 1 that, by convention, $f_{A,\alpha} < f_{A,\beta}$), and $\bar{f}_A$ is restricted to lie between 0.3 and 0.7. Since $D_r(x)$ is symmetric about $x = 0.5$, only half of the blend composition range is shown in Figure 4 to demonstrate that, as $\Delta f$ increases from zero (the abscissa), $D_r$ increases as $x$ deviates from unity (or zero). The magnitude of the maximum in $D_r$ at $x = 0.5$ [$\epsilon$, where $\epsilon = (D_r - 1) \times 100\%$] is presented as a function of $\Delta f$ in the inset of Figure 4 and is seen to increase nonlinearly from 0.0 (at $\Delta f = 0.0$) to ≈12.5% (at $\Delta f = 0.4$). An important point regarding these predictions is that they correspond to *both* of the cases described above. That is, $D_r(x)$ is only dependent on $\Delta f$, the difference between $f_{A,\alpha}$ and $f_{A,\beta}$, and not on $f_{A,\alpha}$ and $f_{A,\beta}$ individually, in the strong-segregation regime.

The same is not true, however, for $L_{A,r}$, provided as a function of $x$ in Figure 5. As seen in this figure, predicted $L_{A,r}$ are sensitive to the characteristics of the two case examples examined here, with the (ii) blends ($f_{A,\alpha} = 0.3$) exhibiting larger $L_{A,r}$ than the (i) blends ($f_{A,\alpha} + f_{A,\beta} = 1$) of identical $\Delta f$. Another apparent difference between the predictions for $D_r(x)$ in Figure 4 and $L_{A,r}(x)$ in Figure 5 is that, for $\Delta f > 0$, predicted $L_{A,r}$ increase

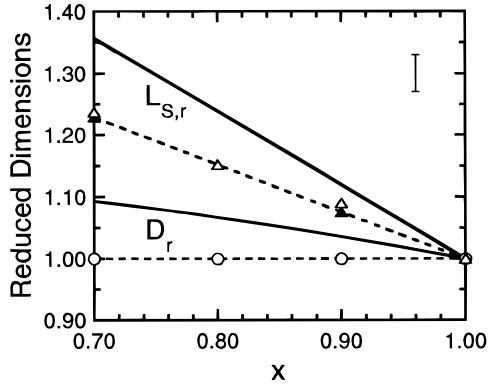


**Figure 6.** Comparison of experimental data ($f_{A,\alpha} = 0.46$, $f_{A,\beta} = 0.83$, and $\Delta f = 0.37$) and theoretical predictions for $D_r$ and $L_{S,r}$. Experimental data points, $D_r$ (circles) and $L_{S,r}$ (triangles), are derived from SAXS (open symbols) and TEM (filled symbols) measurements, whereas corresponding predictions from the strong-segregation formalism developed here are displayed as solid lines. The error bar (upper right corner) provides a measure of uncertainty in the SAXS data.

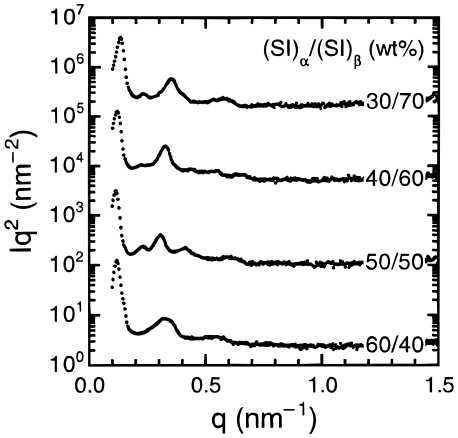


**Figure 7.** Series of SAXS profiles corresponding to (from bottom to top) the 60/40, 50/50, 40/60, and 30/70 $\alpha/\beta$ blends. As $X$ decreases (and $\langle f_S \rangle$ increases), the blends undergo a transition from a bicontinuous morphology (60/40) to hexagonal morphologies (50/50 to 30/70).

monotonically from unity with decreasing $x$. That is, while $D_r(x)$ curves are symmetric about, and display a maximum at, $x = 0.5$, each $L_{A,r}(x)$ curve reaches a maximum at $x = 0.0$. This behavior is consistent with the arbitrary convention established in Figure 1, namely, $f_{A,\alpha} < f_{A,\beta}$, in which case the neat α copolymer possesses a shorter A block than the $\beta$ copolymer. Addition of $\beta$ copolymer to the α copolymer results in an increase in the width of the A lamellae due to an increase in the number of resident A monomers. The maximum in $L_{A,r}(x)$ must therefore occur when $\bar{f}_A = \bar{f}_{A,\beta}$, in the limit of pure $\beta$ ($x = 0.0$).

In Figure 6, A is taken to correspond to S so that experimental and predicted values of $D_r$ and $L_{S,r}$ can be compared for the lamellar $\alpha/\beta$ blends ($0.7 \leq x \leq 1.0$) examined in this study. Since only the neat α copolymer is lamellar, the microstructural dimensions of interest must be normalized with respect to those of the α copolymer; i.e., $D_r = D_{\alpha\beta}/D_\alpha$ and $L_{S,r} = L_{S,\alpha\beta}/L_{S,\alpha}$, where $L_{S,\alpha\beta} = \langle f_S \rangle D_{\alpha\beta}$ from SAXS measurements. Recall from section I that $f_{S,\alpha}$ and $f_{S,\beta}$ (needed for evaluation of $\Psi$ and $\bar{f}_S$, and consequently $D_r$ and $L_{S,r}$) are about 0.46 and 0.83, respectively, in which case $\Delta f = 0.37$. As is evident from Figure 6, $D_r$ and $L_{S,r}$ obtained from the strong-segregation formalism developed here clearly overpredict the reduced SAXS data (by as much as 10% at $x = 0.7$). Three important points must be remembered at this juncture. The first is that the uncertainty in the SAXS data is about 3%, while that in the TEM data is as much as ≈4%. While such uncertainty does not solely account for the difference between theoretical predictions and experimental data, it must be considered in this comparison. The second is that, while $N_\alpha$ and $N_\beta$ are comparable in magnitude in the present study, they are not identical, as required in the theoretical formalism proposed here.

Thirdly, the framework presented in this work assumes strong-segregation behavior in the limit as $\chi N \rightarrow \infty$. With molecular weights of 80 000 each, the α and $\beta$ copolymers (and, hence, their blends) possess finite $\chi N$ values and reside in either the intermediate- or strong-segregation regime, which is more accurately described by SCF theory. Due to the assumption of a single chain trajectory along the lamellar normal in strongly-segregated block copolymers,[20,37,39−41] lateral microstructural dimensions (e.g., $D$) predicted from strong-segregation formalisms tend to be larger than those obtained from SCF frameworks. Matsen,[39] for instance, reports that predicted $D$ for symmetric copolymer blends ($\Delta f = 0$ and $N_\alpha > N_\beta$) in the strong-segregation approximation consistently exceed those obtained from SCF analysis (by as much as about 10% when $N_\beta/N_\alpha = 0.25$). An interesting feature of Figure 6 is that $D_r$ from SAXS measurements are invariant with respect to $x$, while predicted $D_r$ in the strong-segregation limit increase monotonically (over $0.7 \leq x \leq 1.0$) as $x$ decreases from unity.

**III. Blends Possessing Nonlamellar Morphologies. A. Conventional SAXS/TEM Analyses.** A series of SAXS profiles obtained from the 60/40, 50/50, 40/60, and 30/70 blends is shown in Figure 7 and, unlike the profiles seen in Figure 2, reveals an evolution in morphology as the blends go from being α-rich to $\beta$-rich. Corresponding changes in morphology with blend composition are likewise evident in the electron micrographs presented in Figure 8. The SAXS profile corresponding to the 60/40 blend, for instance, is weakly similar to profiles previously reported for ordered bicontinuous morphologies, such as the G*.[8,43] One of the scattering characteristics of this cubic bicontinuous morphology is the existence of peaks at spacing ratios of $\sqrt{3}:\sqrt{4}$, typically appearing as an intense peak immediately followed by a secondary peak or discrete shoulder, depending on instrument resolution. A high-resolution SAXS profile obtained from the 60/40 blend is presented in Figure 9a. A shoulder appears on the outside of the principal reflection at an approximate position ratio of $\sqrt{8}/6$ with respect to the lowest diffraction order, consistent with the cubic microstructural assignment. The incoherent signal extending from $q = 0.24$ to 0.36 $nm^{-1}$ obscures any coherent scattering in this range, although poorly resolved reflections might be present in the vicinity of $q = 0.24$ $nm^{-1}$; this would correspond to peaks at position ratios between $\sqrt{20}$ and $\sqrt{28}$, if the principal reflection is assigned $\sqrt{6}$. A strong reflection appears at a position ratio of $\sqrt{54}$, or 3 times the spacing of the principal reflection. As such a strong peak is not normally seen at this position in diffraction from the G* morphology, this feature might indicate the coexistence of a poorly ordered cubic phase with a layered structure of some sort.

Unambiguous identification of the microstructure of this blend is not possible due to the limited number of poorly resolved diffraction orders. An electron micrograph of the 60/40 blend in Figure 8a reveals that the blend morphology is bicontinuous and strikingly

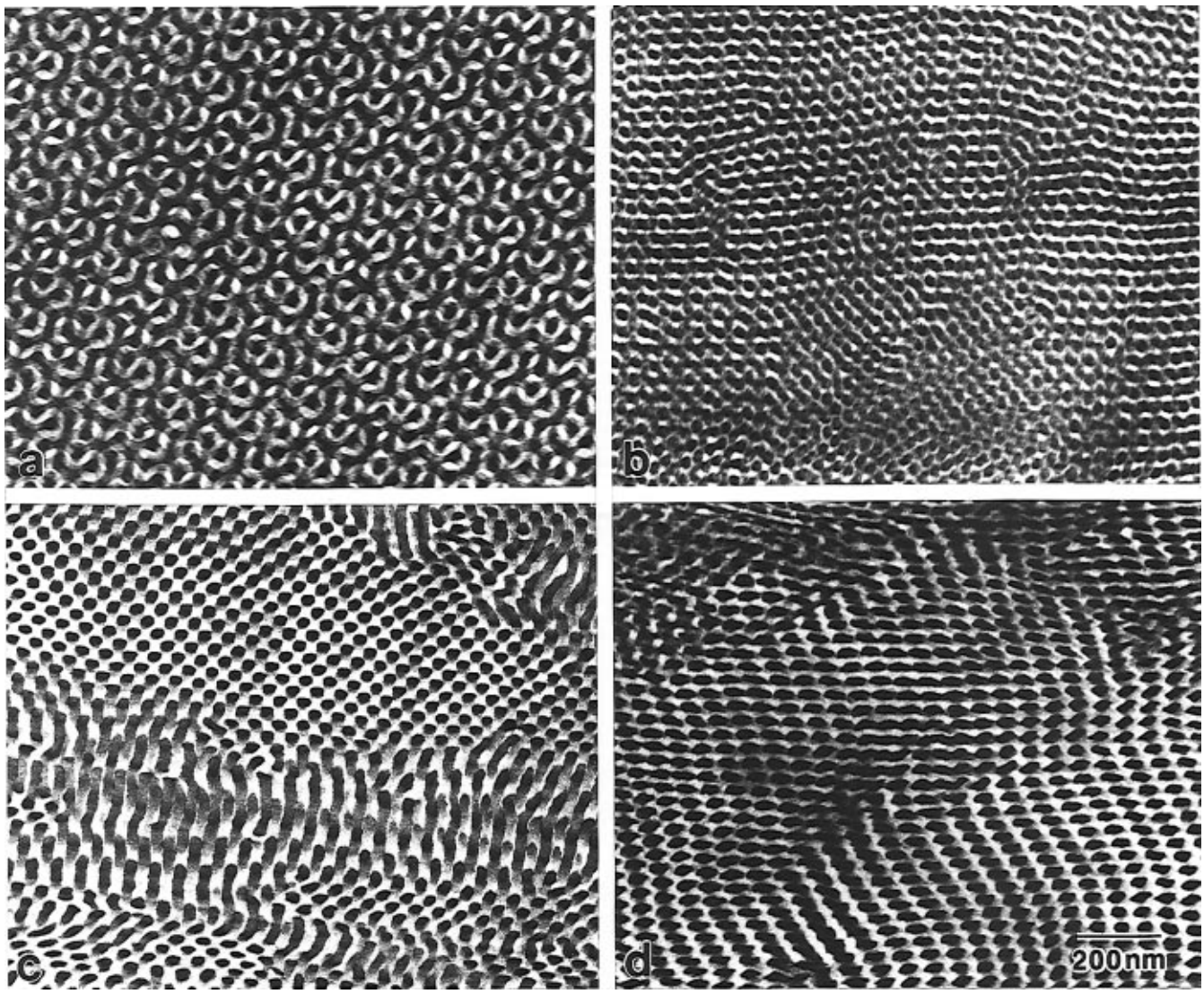


**Figure 8.** Electron micrographs of the four blends described in Figure 7. A projection from the bicontinuous morphology produced in the 60/40 blend is shown along the [111] axis[44,60] in (a), whereas the morphology found in the 50/50 blend is displayed in (b). The cylindrical morphology is clearly evident in the 40/60 (c) and 30/70 (d) blends.

reminiscent of the double-diamond and G* morphologies in projection along the [111] axis[44,60] (Figure 8a). This blend exhibits two important characteristics: (i) the morphology seen in Figure 8a is the only one present and (ii) the morphology is highly oriented, even in the absence of shear-induced alignment.[45] These features both suggest that the α and $\beta$ copolymers are miscible at the molecular level, at least at this composition (61 vol % S, which coincides with the appearance of cubic bicontinuous morphologies in neat starblock copolymers[43,46]). Similar observations have been reported by Schwark,[47] who found that a blend of a lamellar copolymer and a copolymer possessing the cylindrical morphology could yield a bicontinuous morphology. While the thermodynamic stability of bicontinuous morphologies has recently become the subject of immense theoretical interest,[48,49] no attempt is made here to extend the framework proposed in the previous section to blends displaying nonlamellar morphologies.

According to the SAXS profile displayed in Figure 7, the 50/50 blend consists of the cylindrical morphology, as evidenced by the appearance of peaks at spacing ratios of $1:\sqrt{3}:\sqrt{4}$. This is confirmed in the high-resolution profile shown in Figure 9b, although the broad peaks evident in this figure are suggestive of a distorted lattice with relatively little long-range order. In contrast, the corresponding electron micrograph in Figure 8b suggests that this blend consists of coexisting morphologies, one interconnected, possibly bicontinuous, and the other cylindrical. Localized regions of discrete cylindrical microdomains are, for instance, evident in Figure 8b. The absence of a diffraction signature characteristic of a bicontinuous structure despite the highly ordered nature of that phase as seen in the micrographs suggests that this morphology occupies a very small fraction of the sample volume. These data differ from those corresponding to the 40/60 and 30/70 blends, which, according to the SAXS profiles in Figure 7 and the electron micrographs in Figure 8c,d, respectively, consist solely of hexagonally-packed isoprenic cylinders. Comparison of Figure 8c,d to those presented in Figure 3c−f reveals that the cylindrical microdomains in the 40/60 and 30/70 blends are much smaller than those observed in the 80/20 and 70/30 blends. According to measurements obtained from these and similar micrographs, values of $\langle f_S \rangle$ are estimated (±0.02) from the cylindrical (not lamellar) microdomains to be about 0.73 (80/20), 0.65 (70/30), 0.68 (40/60), and 0.70 (30/70), and corresponding values of $\langle f_S \rangle$ calculated from the blend composition are 0.53, 0.57, 0.68, and 0.71, respectively. Thus, the cylindrical morphologies evident in the I-rich (one-phase) blends are consistent with the blend compositions and full $\alpha/\beta$ miscibility, whereas those in the S-rich (two-phase) blends are $\beta$-rich and conse-

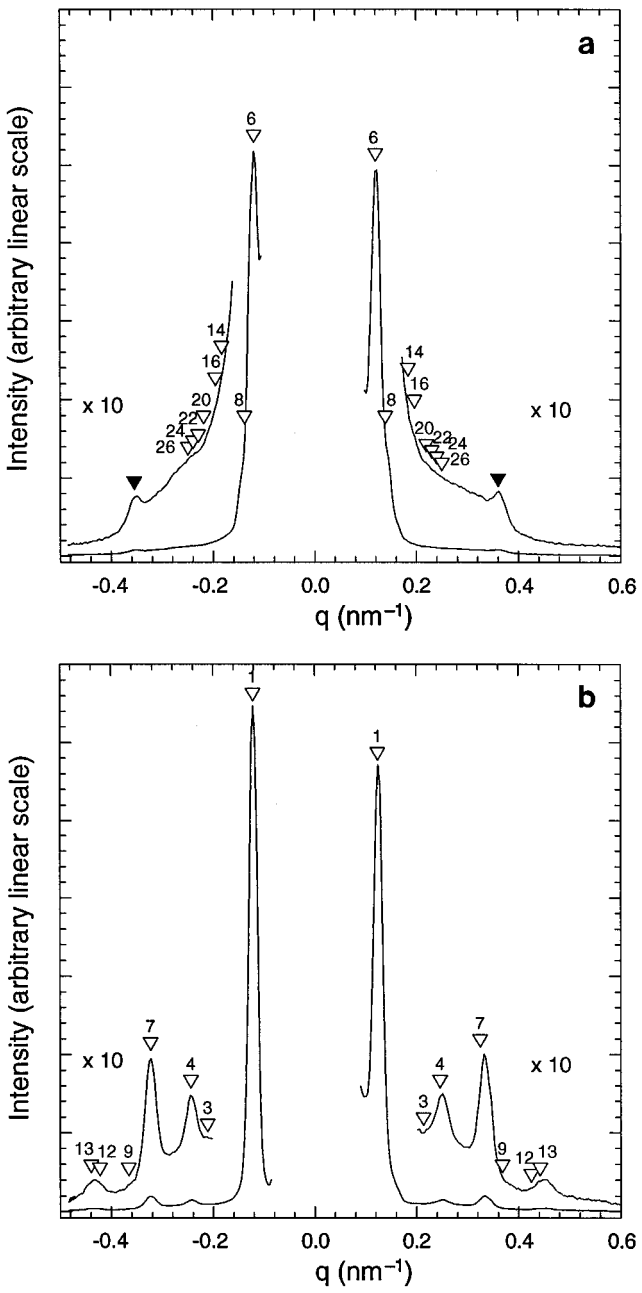


**Figure 9.** High-resolution SAXS profiles obtained from the (a) 60/40 and (b) 50/50 blends. Inverted triangles in (a) indicate expected peak position ratios for the first few orders of the G* morphology; they do not indicate locations where peaks are actually observed. The reflection marked with the unlabeled filled symbol appears at 3× the spacing ratio of the principal diffraction order. Inverted triangles in (b) indicate similar positions for the hexagonally packed cylindrical morphology. The label on each triangle gives the square of the peak position ratio (modulus).

quently reflect a spatially inhomogeneous distribution of copolymers. Again, we note that we are unable to determine whether these spatial inhomogeneities are equilibrium in nature.

**B. Electron Tomographic Analysis.** To reconcile the apparent contradiction between SAXS and TEM concerning the 50/50 blend, as well as examine the cubic bicontinuous morphology in the 60/40 blend, electron tomography has been performed to more carefully scrutinize the three-dimensional microstructures of these blends.

Electron microscopic tomography allows the complete three-dimensional internal structure of an object to be reconstructed from a set of tilted views, without imposing any *a priori* assumptions or requirements regarding the symmetry of the object. This powerful approach has been proven to be extremely valuable in the analysis of complex biological structures such as chromosomes,[50] centrosomes,[51] kinetochores,[52] and cilia.[53] Detailed descriptions of the filtered (*r*-weighted) back-projection imaging technique are available elsewhere,[54−58] and only the general approach and pertinent operating parameters are included here. A series of 49 480 × 480 pixel images of an area of interest from a single TEM section were digitally collected at a resolution of 2.1 nm/pixel using 2× binning on a Thompson 1024 × 1024 CCD chip fiber-optically coupled to a single crystal scintillator. Data were collected at tilt angles ranging from +60° to −60° in 2.5° increments. Examples of the images at six different tilt angles are shown in Figure 10. To minimize radiation damage, specimen exposure to the electron beam was limited to image acquisition and focusing using recently developed automated data collection methods that dynamically track changes in sample position and focus during tilting.[57] The images were first converted to mass density (mass-normalization) and then aligned with respect to fiducial markers (30 nm colloidal gold beads) using a least-squares minimization algorithm.[54] Using the EMCAT reconstruction software package,[58] the 3-D volume was reconstructed from the collected projections. Image display and analysis was conducted using the PRIISM image graphics package.[59]

Two reconstructions were performed, one of the 60/40 blend (with the bicontinuous, probably G*, morphology) and the other of the 50/50 blend (with the hexagonal, cylindrical-like morphology). The mean alignment error ($\sigma$), averaged over all of the fiducial markers (at least 8) used in aligning the images, is shown as a function of tilt angle for the 60/40 and 50/50 blend reconstructions in Figure 11a,b, respectively. Note that the overall mean error is less than the resolution of the collected images. Lateral sample shrinkage, due to electron radiation damage, is estimated to be about 2.7 and 2.1%, respectively, as discerned from the relative positions of the fiducial markers immediately before and after acquisition of the tilt series. Alignment errors (Figure 11) and lateral shrinkage measurements provide a quantitative assessment of radiation-induced specimen damage. The extent of beam damage can also be qualitatively discerned by comparing the morphological features of images collected at 0° tilt before and after the tilt sequence. In this work, such image pairs are virtually indistinguishable. Solid renderings of the reconstructed 60/40 blend morphology are displayed at different orientations from −20° to +200° rotation (in 20° increments) in Figure 12. The bicontinuous cubic morphology in this figure consists of a network of *ca.* 20 nm channels which closely resemble the constant mean-curvature surfaces often employed[8,43,44,60] to simulate two-dimensional (TEM) projections of complex cubic morphologies. Note, however, that the morphology seen in Figure 12 cannot be readily described by a surface with precise symmetry (and mathematical properties) due to microstructural imperfections. Since the morphology is discerned experimentally, it is representative of a physically real structure, incorporating all of the naturally occurring (and potentially property-limiting) defects associated with microphase ordering.

Even with the irregularities present, it is clear from the reconstructed images displayed in Figure 12 that the 60/40 blend is bicontinuous, although its symmetry group ($Pn\bar{3}m$ for double-diamond *vs* $Ia\bar{3}d$ for G*) cannot be clearly identified. Since these morphologies differ

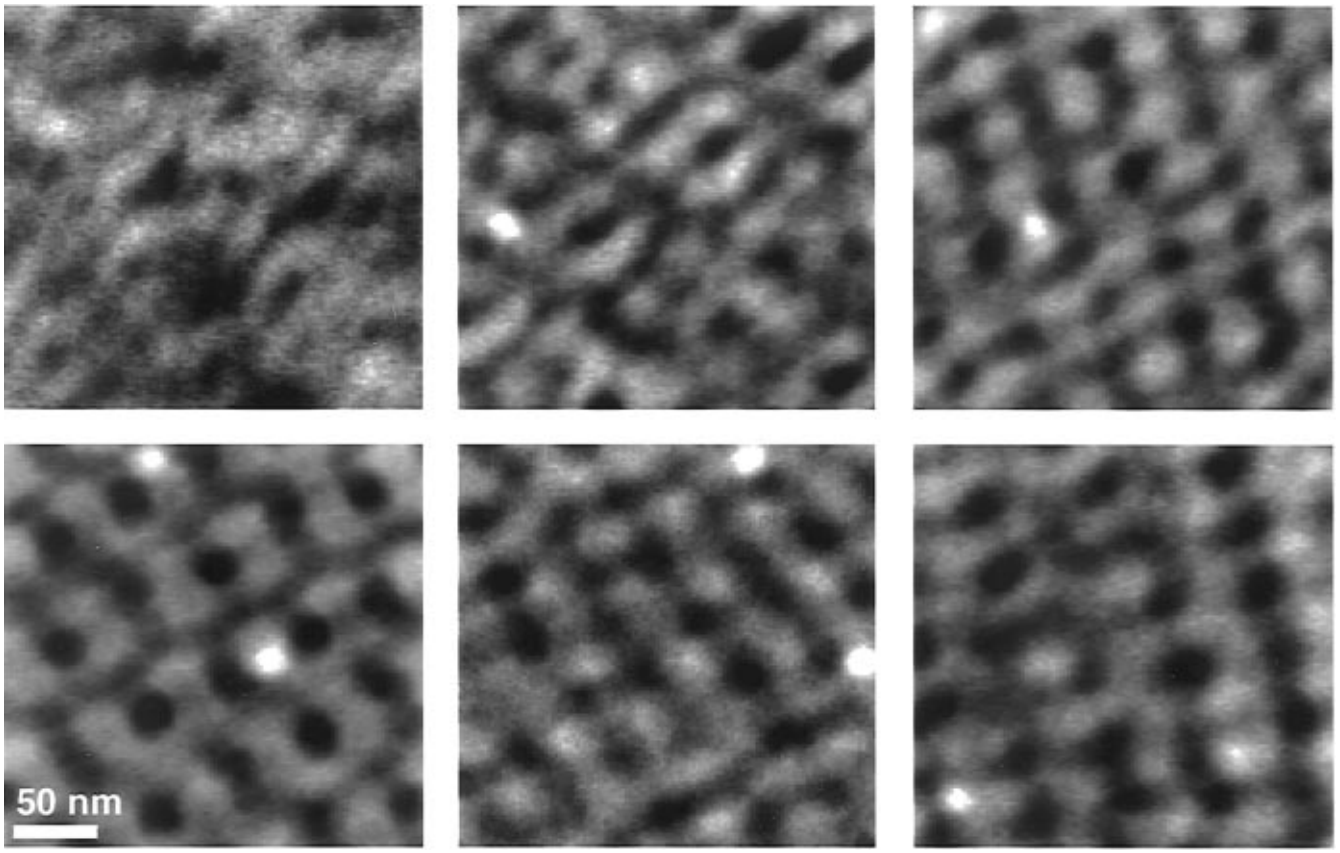


**Figure 10.** Digital electron micrographs of the 60/40 blend collected at six different tilt angles ranging from −45° to +30° in 15° increments from left to right and top to bottom. These images are contrast-reversed, in which case the S and I microphases appear dark and light, respectively.

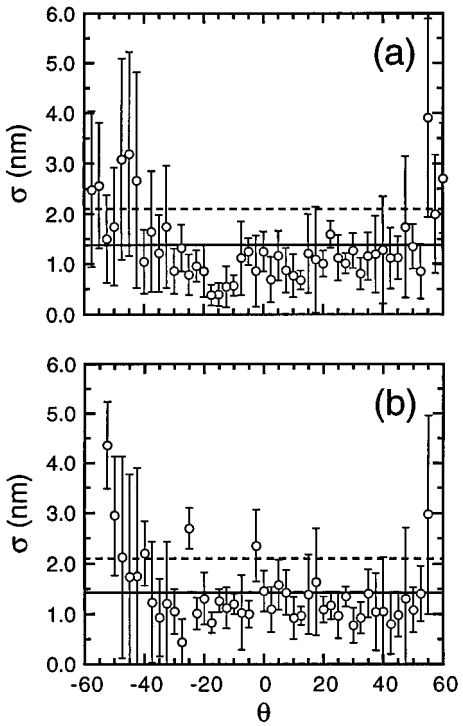


**Figure 11.** Mean error in fiducial marker position ($\sigma$) incurred during alignment of tilt projections for 3-D reconstructions of the (a) 60/40 and (b) 50/50 blends. The vertical lines denote standard deviations in the data, while the solid and dashed lines correspond to the angle-averaged overall error and image resolution (per pixel), respectively.

in the coordination of the minority component channels—the double-diamond network is built from four-connected tetrahedral elements, while the G* structure is based on three-connected channels—differentiation of these phases can be achieved by counting the number of minority component "tubes" which join at a vertex of the reconstructed morphology. From images such as those presented in Figure 12, the number of connected channels intersecting at each vertex is 3. In a related work,[11] the G* morphology has been unambiguously identified by both SAXS and TEM. Figure 13 is a series of two-dimensional images sliced from the reconstructed volume element of the 60/40 blend morphology along two different directions: normal to the electron beam path (small images) and parallel to the electron beam path (large image). If $z$ is perpendicular to the specimen surface, each small image in Figure 13 consists of projected information from an incremental specimen thickness $\Delta z$, where $\Delta z \approx 21$ nm. [Since cryoultramicrotomy routinely produces specimens ranging from 60 to 100 nm in thickness, acquisition of a complete set of comparable images from conventional TEM free of sectioning distortions would be an impossible task.] The large image in Figure 13 shows the TEM specimen in cross-section, with the vertical axis corresponding to the $z$-axis. Upon comparison of the images shown in Figures 12 and 13 to the model surfaces provided in ref 8, the morphology produced in the 60/40 blend is probably G*.

Reconstructed images similar to those provided for the 60/40 blend in Figure 12 are presented in Figure 14 for the 50/50 blend and reveal that this blend consists of hexagonally packed cylinders which appear elliptical, rather than circular, in cross-section (in agreement with the SAXS data presented in Figure 9b). The major and minor elliptical axes measure about 50 and 30 nm, respectively, across. As is evident from the cross-sectional view, some of the cylinders also appear to be connected laterally, suggesting that the morphology may

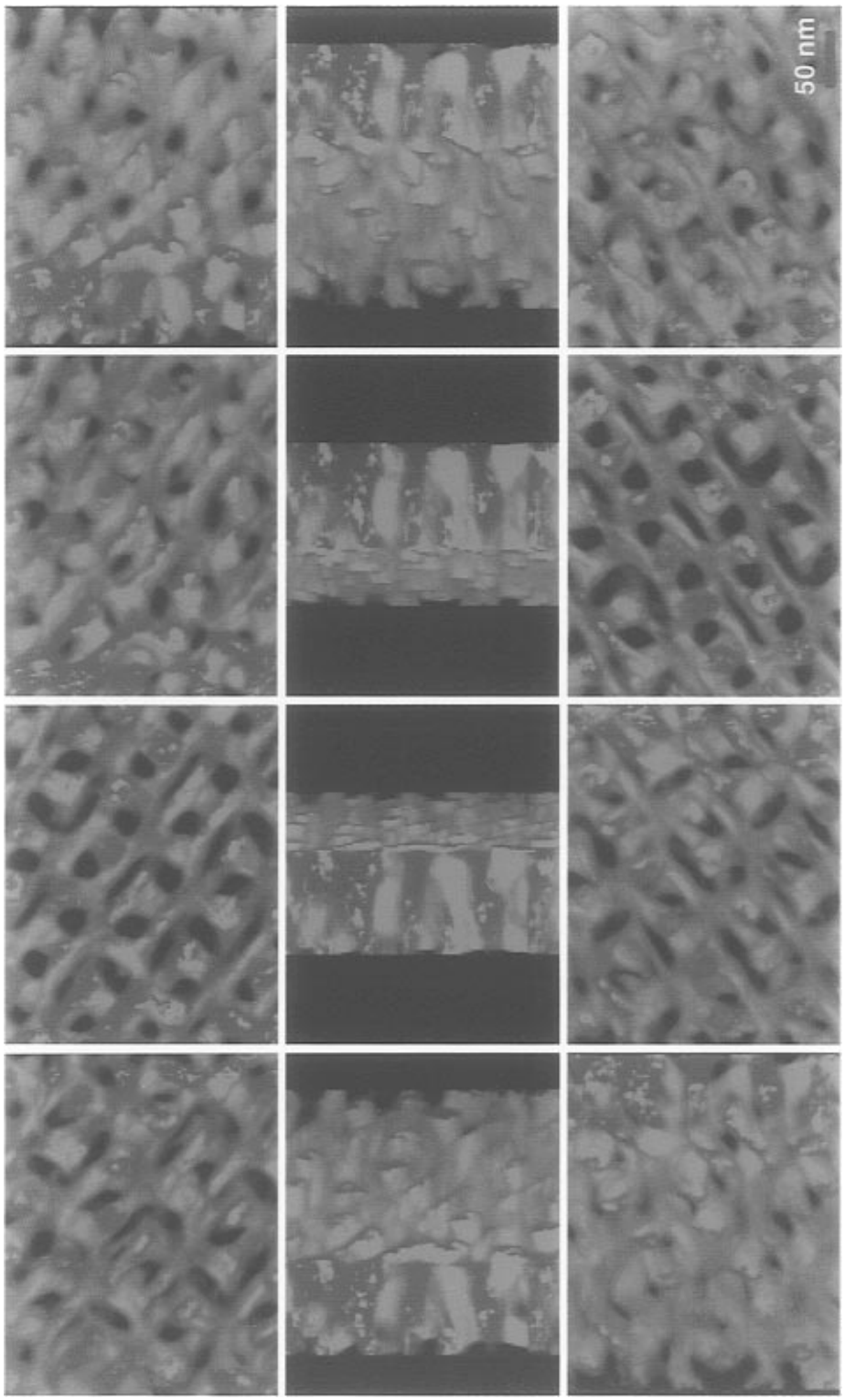


**Figure 12.** Three-dimensional images of the 60/40 blend obtained through electron tomography. Solid renderings are displayed here at rotation angles ranging from −20° to +200° (in 20° increments from left to right and top to bottom) to facilitate visualization of the bicontinuous channel network comprising this morphology. Note that three channels intersect at each vertex.

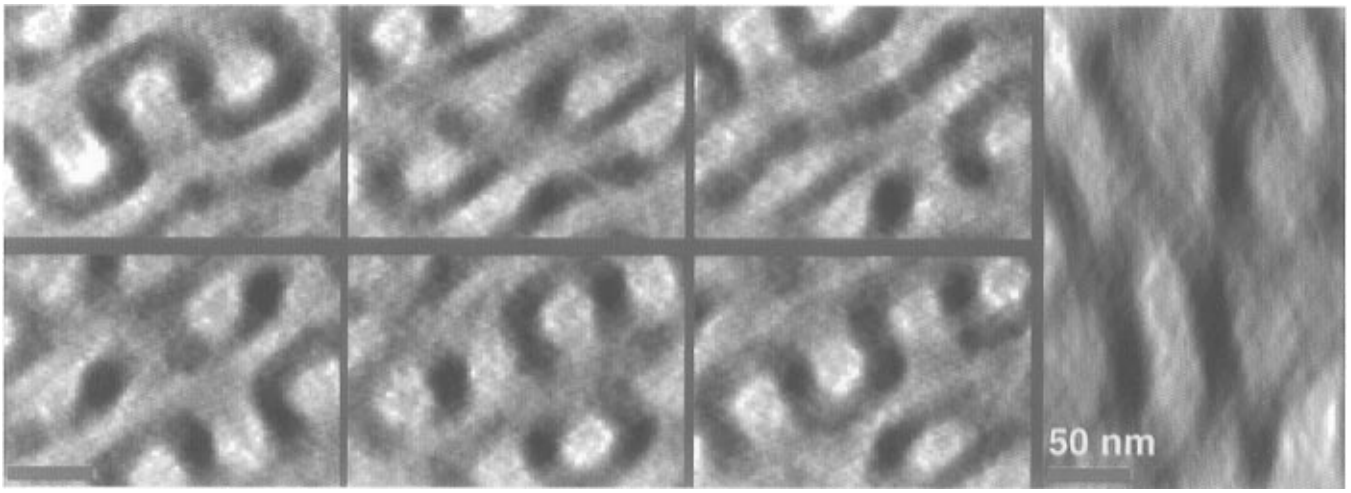


**Figure 13.** Two-dimensional images sliced from the reconstructed morphology presented in Figure 12. The thickness of each contrast-reversed "slice" in the six small images (sequential from left to right and top to bottom) is about 21 nm along the electron beam axis, whereas the large single image is a cross-section of the TEM specimen.

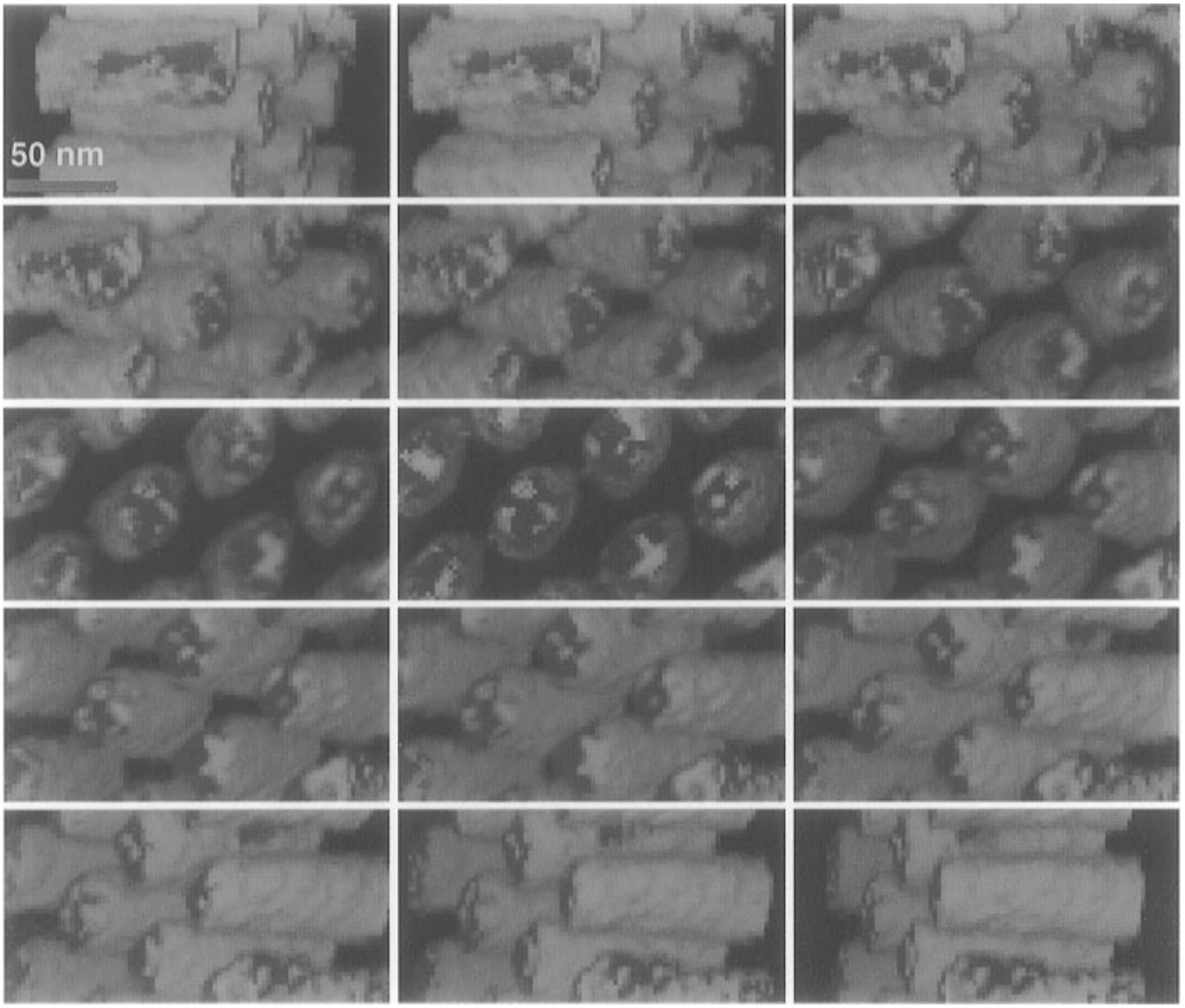


**Figure 14.** Three-dimensional reconstructions of the 50/50 $\alpha/\beta$ blend demonstrating that the morphology consists of hexagonally packed cylindrical microdomains which appear elliptical in cross-section. The images are rotated from $-70°$ to $+70°$ in 10° increments (left to right and top to bottom). Some of the cylinders are laterally connected, suggesting that this morphology may be related to the hexagonal "channel" morphologies recently reported.[6]

be related to one of the "channel" morphologies proposed by Hamley *et al.*[6] To ensure that the images in Figures 12 and 14 are representative of the microstructure in the 60/40 (Figure 12) and 50/50 (Figure 14) blends, the pixel levels in these solid reconstructions have been thresholded so that $\langle f_S \rangle$ lies between 0.50 and 0.65

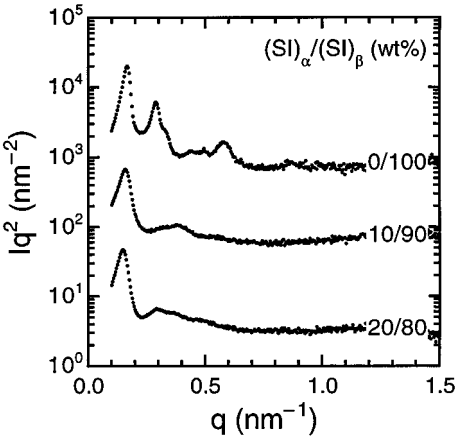


**Figure 15.** Scattering profiles obtained from the 20/80 (bottom), 10/90 (middle), and 0/100 (top) blends. Patterns corresponding to the two $\beta$-rich blends indicate the absence of higher-order scattering maxima, suggesting that the morphologies do not possess long-range order. The $\beta$ copolymer exhibits a spherical morphology according to the SAXS profile shown here.

(values of $\langle f_S \rangle$ estimated from the known blend composition are 0.61 and 0.64, respectively). A notable feature of the microstructure in Figure 14 is the highly aligned nature of the major axes of the ellipses. Such alignment is unlikely to be microstructural in origin, considering the 6-fold rotational degeneracy of the underlying hexagonal lattice. Instead, it may have been induced by the sample preparation process. However, we note that the hexagonal lattice does not appear highly distorted (as it would upon mechanical deformation during microtomy) and that the microstructural elements are best described as elliptical in cross-section.

**IV. Styrene-Rich Blends Possessing Cubic Morphologies.** Further reduction in the isoprene concentration induces a transition from the cylindrical morphology to an irregular (possibly bicontinuous) morphology, as seen in the SAXS profiles provided in Figure 15 and the electron micrographs in Figure 16. This morphology, apparent in the 20/80 and 10/90 blends, is characterized by the absence of well-defined higher-order scattering reflections (Figure 15) and by the presence of highly interconnected isoprenic microdomains (see Figures 16a,b). It is similar in appearance to the "mesh" (or "strut") morphology reported by Hashimoto *et al.*,[61] and can be envisioned as an intermediate morphology comprised of randomly oriented, short stubby cylinders. Such morphologies have been observed[62] in aqueous surfactant systems at compositions between those yielding the cylindrical (hexagonal) and spherical (cubic) morphologies. The neat $\beta$ copolymer (0/100) consists principally of dispersed isoprenic spheres on a body-centered cubic (BCC) lattice, as identified by the scattering reflections at $1:\sqrt{3}:\sqrt{4}:\sqrt{7}:\sqrt{12}$ in Figure 15 and the micrograph in Figure 16c.

As this study has demonstrated, blends comprised of two ordered diblock copolymers with dissimilar compositions (and morphologies) can be used to alter, and ultimately control, copolymer morphology and microstructural dimensions (see Table 1). As noted earlier, $D$ from the lamellar and bicontinuous (intermediate) morphologies remains nearly constant, and then decreases by as much as 28% when $X$ drops below 50% α (and the blends become isoprene-rich). In contrast, $L_S$ increases with decreasing $X$, reflecting the existence of swollen S lamellae in asymmetric lamellar $\alpha/\beta$ blends. Note that the blend composition corresponding to the bicontinuous morphology ($\langle f_S \rangle \approx 0.61$) is in excellent

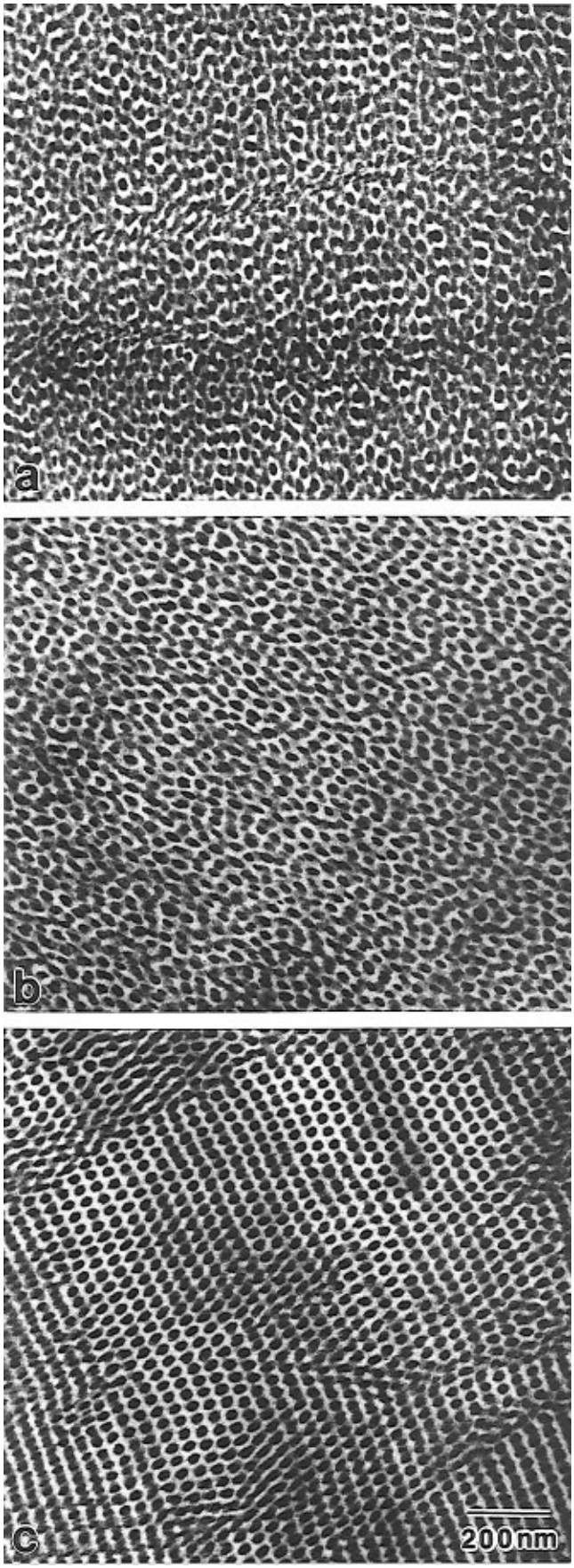


**Figure 16.** Series of electron micrographs imaged from the blends described in Figure 15. As expected from the corresponding SAXS profiles, the (a) 20/80 and (b) 10/90 blends exhibit an irregular morphology which, from these projections, consists of dispersions and an interconnected network, whereas the neat $\beta$ copolymer (c) is comprised principally of dispersed isoprenic spheres.

**Table 1. Microstructural Dimensions and Morphologies of the $(SI)_\alpha/(SI)_\beta$ Blends Examined Here**

| $X$ | $W_S$ | $\langle f_S \rangle^a$ | $D^b$ (nm) | $D^c$ (nm) | $L_S{}^d$ (nm) | $L_S{}^e$ (nm) | morphology |
|---|---|---|---|---|---|---|---|
| 100 | 0.50 | 0.46 | 53.2 | 48.5 | 24.5 | 24.7 | lamellar |
| 90 | 0.53 | 0.50 (0.49) | 53.2 | 48.5 | 26.7 (26.1) | 26.6 | lamellar |
| 80 | 0.57 | 0.53 | 53.2 | 48.5 | 28.2 | 28.4 | lamellar/cylindrical |
| 70 | 0.61 | 0.57 (0.56) | 53.2 | 48.5 | 30.3 (29.8) | 30.3 | lamellar/cylindrical |
| 60 | 0.64 | 0.61 (0.60) | 53.2 | | | | bicontinuous (G*) |
| 50 | 0.68 | 0.64 | 53.2 | | | | (elliptical) cylindrical |
| 40 | 0.71 | 0.68 (0.67) | 50.3 | | | | cylindrical |
| 30 | 0.75 | 0.72 (0.71) | 47.6 | | | | cylindrical |
| 20 | 0.78 | 0.75 | 43.1 | | | | (irregular) mesh |
| 10 | 0.82 | 0.79 | 39.3 | | | | (irregular) mesh |
| 0 | 0.85 | 0.83 | 37.7 | | | | spherical |

[a] Calculated at 25 °C (100 °C) using the densities given in the text. [b] Determined from the principal peak position in SAXS patterns (±3% for lamellae). [c] Measured from 2-D Fourier-transformed TEM images (±3%). [d] Calculated from $\langle f_S \rangle D$ at 25 °C (100 °C). [e] Measured from digital TEM images in Digital Micrograph (±4%).

agreement with that yielding the G* morphology in neat starblock copolymers.[43,46] This comparison suggests that binary copolymer blends behave more like neat copolymers than do copolymer/homopolymer blends,[14−16] in which microphase bicontinuity arises when $\langle f_S \rangle$ lies between 0.65 and 0.67. As $X$ is increased further, the bicontinuous morphology gives way first to isoprenic cylinders and then to a (mesh-like) morphology lacking long-range periodic order. As $X \rightarrow 0$, the spherical morphology characteristic of the $\beta$ copolymer is recovered. Such physical, rather than chemical, synthesis[24] provides an ideal opportunity to study the conformational properties of mixtures of bimodal distributions of grafted polymer chains confined to nanoscale microstructures with and without curvature.[63]

## Conclusions

While previous efforts have focused on controlling block copolymer morphology through the addition of a parent homopolymer, the SAXS and TEM results presented here indicate that blends of two strongly segregated copolymers possessing dissimilar morphologies can effectively be used to produce intermediate morphologies which are more representative of neat copolymers of equivalent bulk composition. Addition of an asymmetric $\beta$ copolymer exhibiting isoprenic dispersions to a symmetric $\alpha$ copolymer initially induces swelling of the styrenic lamellae, the extent of which can be reasonably well-predicted by a strong-segregation formalism proposed here for compositionally heterogeneous lamellar copolymer blends. As the concentration of $\beta$ is increased further, coexisting grains of cylinders are observed to form within a lamellar matrix, suggesting that macrophase separation occurs between the $\alpha$ and $\beta$ copolymers even though the molecular weights of the constituent copolymers are comparable. If the coexisting morphologies are equilibrium in nature, developing from an initially isotropic distribution of the blend components, this phase separation arises as a consequence of this coexistence. In some cases, the cylindrical grains are extremely small, consisting of only a few (<10) microdomains. Upon further addition of $\beta$, a well-oriented bicontinuous morphology develops, followed by a hexagonal intermediate morphology comprised of elliptical (and sometimes connected) cylinders. Electron microscopic tomography has been employed here to provide the first three-dimensional images of these morphologies at high spatial resolution. Observed morphologies in $\beta$-rich blends include the classical cylindrical morphology and a disordered bicontinuous morphology. These results demonstrate that binary block copolymer blends can be used to generate intermediate morphologies, without resorting to tailored chemical synthesis, and provide valuable insight into the molecular mixing of spatially confined chains grafted to a repulsive interface.

**Acknowledgment.** This study has been supported by the Petroleum Research Fund, administered by the American Chemical Society, the National Science Foundation (CMS-941-2361), and the Director, Office of Energy Research, Office of Basic Energy Sciences, Materials Science Division of the U.S. Department of Energy under contract DE-AC03-76SF00098. R.J.S. thanks the National Center for Electron Microscopy for a Visiting Scientist Fellowship and Drs. K. M. Krishnan and U. Dahmen for valuable discussions. Work at Princeton University was supported by the U.S. Department of Energy under contract DE-FG02-87ER60522 and the National Science Foundation (DMR-922-3966). Funding for D.A.A., J.W.S., M.B.B., and J.C.F. was provided by the Howard Hughes Medical Institute and the National Institute of Health (GM31627, D.A.A.; GM25101, J.W.S.). We are grateful to Mr. H. Chen (UCSF), Mr. J. T. Grothaus (P&G), and Mr. M. A. Burchfield (P&G) for technical assistance.

## References and Notes

(1) Leibler, L. *Macromolecules* **1980**, *13*, 1602.
(2) Fredrickson, G. H.; Bates, F. S. *Annu. Rev. Phys. Chem.* **1990**, *41*, 525.
(3) Hamley, I. W.; Gehlsen, M. D.; Khandpur, A. K.; Koppi, K. A.; Rosedale, J. H.; Schulz, M. F.; Bates, F. S.; Almdal, K.; Mortensen, K. *J. Phys. II* **1994**, *4*, 2161.
(4) Gehlsen, M. D.; Bates, F. S. *Macromolecules* **1994**, *27*, 3611.
(5) Thomas, E. L.; Anderson, D. M.; Henkee, C. S.; Hoffman, D. *Nature* **1988**, *334*, 598.
(6) Hamley, I. W.; Koppi, K. A.; Rosedale, J. H.; Bates, F. S.; Almdal, K.; Mortensen, K. *Macromolecules* **1993**, *26*, 5959.
(7) Förster, S.; Khandpur, A. K.; Zhao, J.; Bates, F. S.; Hamley, I. W.; Ryan, A. T.; Bras, W. *Macromolecules* **1994**, *27*, 6922.
(8) Hajduk, D. A.; Harper, P. E.; Gruner, S. M.; Honeker, C. C.; Kim, G.; Thomas, E. L.; Fetters, L. J. *Macromolecules* **1994**, *27*, 4063.
(9) Schulz, M. F.; Bates, F. S.; Almdal, K.; Mortensen, K. *Phys. Rev. Lett.* **1994**, *73*, 86.
(10) While existence of the ordered bicontinuous double-diamond (OBDD) morphology has been reported, recent data re-evaluation[40] suggests that such morphologies observed are in fact G*.
(11) Laurer, J. H.; Fung, J. C.; Hajduk, D. A.; Sedat, J. W.; Agard, D. A.; Smith, S. D.; Gruner, S. M.; Spontak, R. J. Manuscript in preparation.
(12) Winey, K. I.; Thomas, E. L.; Fetters, L. J. *Macromolecules* **1991**, *24*, 6182.
(13) Hashimoto, T.; Tanaka, H.; Hasegawa, H. *Macromolecules* **1990**, *23*, 4378. Tanaka, H.; Hasegawa, H.; Hashimoto, T. *Macromolecules* **1991**, *24*, 240.
(14) Winey, K. I.; Thomas, E. L.; Fetters, L. J. *J. Chem. Phys.* **1991**, *95*, 9367.
(15) Winey, K. I.; Thomas, E. L.; Fetters, L. J. *Macromolecules* **1992**, *25*, 422, 2645.
(16) Spontak, R. J.; Smith, S. D.; Ashraf, A. *Macromolecules* **1993**, *26*, 956.

(17) Disko, M. M.; Liang, K. S.; Behal, S. K.; Roe, R.-J.; Jeon, K. J. *Macromolecules* **1993**, *26*, 2983.
(18) Spontak, R. J.; Smith, S. D.; Ashraf, A. *Polymer* **1993**, *34*, 2233.
(19) Shull, K. R.; Winey, K. I. *Macromolecules* **1992**, *25*, 2637.
(20) Banaszak, M.; Whitmore, M. D. *Macromolecules* **1992**, *25*, 2757.
(21) Matsen, M. W. *Phys. Rev. Lett.* **1995**, *74*, 4225; *Macromolecules* **1995**, *28*, 5765.
(22) Turner, D. C.; Gruner, S. M.; Huang, J. S. *Biochemistry* **1992**, *31*, 1356.
(23) Matsen, M. W.; Bates, F. S. *Macromolecules* **1995**, *28*, 7298.
(24) Zhao, J.; Majumdar, B.; Schulz, M. F.; Bates, F. S.; Almdal, K.; Mortensen, K.; Hajduk, D. A.; Gruner, S. M. *Macromolecules* **1996**, *29*, 1204.
(25) Boothroyd, A.; Rennie, A.; Wignall, G. D. *J. Chem. Phys.* **1993**, *91*, 9135.
(26) Fetters, L. J.; Lohse, D. J.; Richter, D.; Witten, T. A.; Zirkel, A. *Macromolecules* **1994**, *27*, 4639.
(27) Melenkevitz, J.; Muthukumar, M. *Macromolecules* **1991**, *24*, 4199. Lescanec, R. L.; Muthukumar, M. *Macromolecules* **1993**, *26*, 3908.
(28) Almdal, K.; Rosedale, J. H.; Bates, F. S.; Wignall, G. D.; Fredrickson, G. H. *Phys. Rev. Lett.* **1990**, *65*, 1112.
(29) Helfand, E.; Wasserman, Z. R. *Macromolecules* **1976**, *9*, 879. See also: Fredrickson, G. H. In *Physics of Polymer Surfaces and Interfaces*; Sanchez, I. C., Ed.; Butterworth-Heinemann: Boston, 1992.
(30) Semenov, A. N. *Sov. Phys. JETP (Engl. Transl.)* **1985**, *61*, 731.
(31) See, for example: Hashimoto, T.; Shibayama, M.; Kawai, H. *Macromolecules* **1980**, *13*, 1237.
(32) Hajduk, D. A.; Gruner, S. M.; Rangarajan, P.; Register, R. A.; Fetters, L. J.; Honeker, C.; Albalak, R. J.; Thomas, E. L. *Macromolecules* **1994**, *27*, 490.
(33) Hashimoto, T.; Yamasaki, K.; Koizumi, S.; Hasegawa, H. *Macromolecules* **1993**, *26*, 2895.
(34) While nonequilibrium artifacts could be avoided with parent SI copolymers of low molecular weight, the resultant blends would be of less practical interest due to reductions in $\chi N$ and bulk strength.
(35) Shi, A. C.; Noolandi, J.; Hoffmann, H. *Macromolecules* **1994**, *27*, 6661.
(36) Shi, A. C.; Noolandi, J. *Macromolecules* **1994**, *27*, 2936.
(37) Spontak, R. J. *Macromolecules* **1994**, *27*, 6363.
(38) Dan, N.; Safran, S. A. *Macromolecules* **1994**, *27*, 5766.
(39) Matsen, M. W. *J. Chem. Phys.* **1995**, *103*, 3268.
(40) Zhulina, E. B.; Halperin, A. *Macromolecules* **1992**, *25*, 5730.
(41) Jones, R. L.; Kane, L.; Spontak, R. J. *Chem. Eng. Sci.* **1996**, *51*, 1365.
(42) Vilesov, A. D.; Floudas, G.; Pakula, T.; Melenevskaya, E. Yu.; Birshtein, T. M.; Lyatskaya, Yu. V. *Macromol. Chem. Phys.* **1994**, *195*, 2317.
(43) Hajduk, D. A.; Harper, P. E.; Gruner, S. M.; Honeker, C. C.; Thomas, E. L.; Fetters, L. J. *Macromolecules* **1995**, *28*, 2570.
(44) Burger, C.; Antonietti, M.; Ruland, W. *J. Chem. Phys.*, submitted for publication.
(45) Albalak, R. J.; Thomas, E. L. *J. Polym. Sci., Polym. Phys. Ed.* **1993**, *31*, 37; **1994**, *32*, 341.
(46) Thomas, E. L.; Alward, D. B.; Kinning, D. J.; Martin, D. C.; Handlin, D. L.; Fetters, L. J. *Macromolecules* **1986**, *19*, 2197.
(47) Schwark, D. W. Ph.D. Dissertation, University of Massachusetts at Amherst, 1991.
(48) Olmsted, P. D.; Milner, S. T. *Phys. Rev. Lett.* **1994**, *72*, 936.
(49) Matsen, M. W.; Schick, M. *Phys. Rev. Lett.* **1994**, *72*, 2660.
(50) Horowitz, R. A.; Agard, D. A.; Sedat, J. W.; Woodcock, C. L. *J. Cell Biol.* **1994**, *125*, 1.
(51) Moritz, M.; Braunfeld, M. B.; Fung, J. C.; Sedat, J. W.; Alberts, B. M.; Agard, D. A. *J. Cell Biol.* **1995**, *130*, 1149.
(52) McEwen, B. F.; Arena, J. J.; Frank, J.; Rieder, C. L. *J. Cell Biol.* **1993**, *120*, 301.
(53) McEwen, B. F.; Radermacher, M.; Rieder, C. L.; Frank, J. *Proc. Natl. Acad. Sci. U.S.A.* **1986**, *83*, 9040.
(54) Frank, J., Ed. *Electron Tomography: Three-Dimensional Imaging with the Transmission Electron Microscope*; Plenum: New York, 1992.
(55) Bates, R. H. T.; McDonnell, M. J. *Image Restoration and Reconstruction*; Clarendon: Oxford, U.K., 1986.
(56) Spontak, R. J.; Williams, M. C.; Agard, D. A. *Polymer* **1988**, *29*, 387.
(57) Köster, A. J.; Braunfeld, M. B.; Fung, J. C.; Abbey, C. K.; Han, K. R.; Liu, W.; Chen, H.; Sedat, J. W.; Agard, D. A. *Microsc. Soc. Am. Bull.* **1993**, *23*, 176.
(58) Fung, J. C.; Liu, W.; deRuijter, W. J.; Chen, H.; Abbey, C. K.; Sedat, J. W.; Agard, D. A. *J. Struct. Biol.*, in press.
(59) Chen, H.; Swedlow, J. R.; Grote, M.; Sedat, J. W.; Agard, D. A. In *Handbook of Biological Confocal Microscopy*; Pawley, J. B., Ed.; Plenum Press: New York, 1995.
(60) Anderson, D. M.; Bellare, J.; Hoffman, J. T.; Hoffman, D.; Gunther, J.; Thomas, E. L. *J. Colloid Interface Sci.* **1992**, *148*, 398.
(61) Hashimoto, T.; Koizumi, S.; Hasegawa, H.; Izumitani, T.; Hyde, S. T. *Macromolecules* **1992**, *25*, 1433.
(62) Laughlin, R. G. *The Aqueous Phase Behavior of Surfactants*; Academic: London, 1994. Safran, S. A. In *Micelles, Membranes, Microemulsions, and Monolayers*; Gelbart, W. M., Ben-Shaul, A., Roux, D., Eds.; Springer-Verlag: New York, 1994. See also: Luzzati, V.; Vargas, R.; Mariani, P.; Gulik, A.; Delacroix, H. *J. Mol. Biol.* **1993**, *229*, 541.
(63) Birshtein, T. M.; Lyatskaya, Yu. V.; Zhulina, E. B. *Polymer* **1990**, *31*, 2185. Zhulina, E. B.; Birshtein, T. M. *Polymer* **1991**, *32*, 1299. Lai, P.-Y.; Zhulina, E. B. *Macromolecules* **1992**, *25*, 5201.

MA9515689